Composites Science and Technology 247 (2024) 110392

Contents lists available at ScienceDirect

Composites Science and Technology

journal homepage: www.elsevier.com/locate/compscitech

A comparative analysis of acoustic emission sensor embedding in glass fibre composite

Noor Salam Ghadarah *, David Ayre

School of Aerospace, Transport and Manufacturing, Cranfield University, Bedford, MK43 0AL, UK

A B S T R A C T

The manufacturing process of composite structures permits fully embedding acoustic emission (AE) sensors. While the embedding process may pose challenges, its advantages, if proven, can outweigh the challenges. The increased sensitivity resulting from embedding acoustic emission sensors in composites is still not definitively established. A test was set up with pre-determined AE initiation locations (surface and sub-surface) and pre-determined receiving sensor's location (surface and sub-surface) to ensure any sensitivity increase was evident. The receiving sensor's attenuation along (at 90°) and across the fibres (at 45°) was assessed using two test methods: pencil lead breaking (PLB) and actuator methods. The actuator method involved using two pulse generators, the TGP110 pulse generator and the Mistras FieldCal. A range of specific frequencies were utilised, 30, 60, 150 and 300 kHz, using the FieldCal. The results obtained from the test methods were not in agreement with each other. For example, comparing the sensitivity using surface cracks, the PLB method showed decreased sensitivity when embedding the receiving sensor compared to the actuator method, which demonstrated minimal changes in sensitivity. The research aims to clarify the sensitivity increase obtained when embedding an AE sensor while taking into account the crack's position and frequency.

1. Introduction

The use of acoustic emission in composites has been explored for many industries, including automotive [1], energy (wind turbine blades) [2], aerospace [3], liquid rocket motor casing [4] and hydrogen tank [5]. The method's valuable capability lies in detecting and identifying the crack location in a composite without external stimulation or excitation. Despite the challenges posed by the composite's anisotropic properties in locating the AE source, numerous studies have been undertaken to devise solutions [6] [–] [8]. In a composite, the type of crack can be determined due to the unique waveform produced by each failure mode [9] [–] [15].

The ability to embed an acoustic emission sensor is particularly relevant for composites, given the manufacturing process involved. Piezoelectric sensors such as lead zirconate titanate (PZT) and polyvinylidene fluoride (PVDF) can be embedded due to their low thickness. There are both benefits and challenges associated with the integration of AE sensors. Benefits include the theoretical high sensitivity, protection from environmental factors such as foreign objects and external noise, and eliminating the need for a couplant. However, several drawbacks are present, such as the mechanical properties loss associated with embedding, the manufacturing process's complexity, and the inability to incorporate on existing structures.

Several experiments have been conducted to investigate the utilisation of embedded acoustic emission sensors in various composites [9,10,16–23]. The mechanical properties deterioration due to embedding a foreign object is found to be dependent on multiple aspects, including the type of load exerted [24]. The enhanced sensitivity of the embedded acoustic emission sensor varies among researchers and is still open for investigation. This study considers the significance of the crack's frequency and initiation location, aspects that may be neglected but still hold importance.

This study aims to investigate the sensitivity of the embedded sensor, considering the relative position of the crack in relation to the sensor placement as well as the influence of frequency on the sensor's sensitivity.

2. Methodology

2.1. Sensors

A piezoelectric element (PZT) obtained from Farnell (7BB-15-6) was employed as the actuator. The actuator had a diameter of 15 mm and a thickness of 0.22 mm. The PZT receiving sensor, obtained from Farnell (MCFT-15T-4.0A1-121), had dimensions of 15 mm in diameter and 0.13 mm in thickness.

* Corresponding author.
E-mail addresses: n.ghadarah@cranfield.ac.uk (N.S. Ghadarah), d.s.ayre@cranfield.ac.uk (D. Ayre).

https://doi.org/10.1016/j.compscitech.2023.110392
Received 22 August 2023; Received in revised form 16 October 2023; Accepted 7 December 2023
Available online 12 December 2023
0266-3538/© 2023 The Authors. Published by Elsevier Ltd. This is an open access article under the CC BY license (http://creativecommons.org/licenses/by/4.0/).

2.2. Plate manufacturing

The testing plate employed was made of glass fibre-reinforced polymer. The testing plate was fabricated through resin vacuum infusion, incorporating six layers of woven glass fibres, all togeher sandwiched by peel ply. A flow mesh was added to facilitate wetting. The sensors were positioned at the centre of the composite (between the third and fourth ply) when manufacturing the fully embedded actuators plate. The actuators were placed 10, 20 and 30 cm from the receiving sensor along and across the fibres, as shown in Fig. 1B. A copper cable with backing adhesive was utilised to establish the electrical connections. A release film was positioned over the outgoing copper cables.

Four plates were produced – two plates had surface embedded actuators alongside a surface embedded and a fully embedded receiver, as seen in Fig. 2A. The other two plates integrated fully embedded actuators alongside surface embedded and fully embedded receivers, as seen in Fig. 2B.

The fully embedded receivers/actuators were positioned during manufacturing, whereas the surface receivers/actuators were positioned after curing, using the same epoxy. Ultimately, the plate measured 615 mm × 630 mm x 2.6 mm in its final dimensions. The materials used for the manufacturing are detailed in Table 1.

2.3. Equipment

A PCI-2 based AE system (AEwin) was utilised to capture the AE signal from the receiving sensor. The receiving sensor was connected to the AE system using a preamplifier set to a gain of 40 dB. The primary threshold used was 45 dB.

The pulse generator employed was a TGP110 10 MHz model manufactured by Thurlby Thandar Instruments (TTi). It was configured to pulse with a pulse width of 5 μs, a frequency of 4 s and an amplitude of 10 V.

The pencil used for the pencil lead breaking method was from MISTRAS, pre-fitted with a 'shoe'. The pencil lead used had a 0.5 mm diameter and 2H hardness.

The acoustic emission generator, FieldCal by Physical Acoustics, was utilised to generate a specific frequency signal. The amplitude was set to 90 dB, burst to AE, rate to 1 pps and range to 40 dB.

3. Results and discussion

Multiple researchers made significant contributions to identify the effect of fully embedding the acoustic emissions sensor. Researchers have reported a variety of results when embedding the AE sensor, that is: no sensitivity change [20], slight improvement [17] and clear improvement [19]. The testing method used to identify the sensitivity improvement was mechanically testing specimens with and without embedded sensors. Various factors can be attributed to the different outcomes reported, including the sensors, material type, specimen thickness, manufacturing process and mechanical testing (crack location). The mechanical testing method is thought to have a significant effect as the different mechanical tests could give rise to cracks at random locations. Specific mechanical tests, such as the three-point bend test, produce initial surface failure, but cracks can occur from within as the test progresses. On the other hand, the tensile test produces failure at the weakest point, which its location could vary. Also, embedding the acoustic emission sensor within the high-stress regions may introduce failure around the inclusion (sensor), indicating a false increase in sensitivity.

The ability to distinguish the sensor response difference due to the location of a defect will allow the user to verify improvements, if any. The actuating sensors are only present as an artificial crack and will not be present if AE sensors are placed in service. The fully embedded actuators act as a defect from within the composite compared to the surface embedded actuator, representing a defect from the composites' surface.

The receiving sensors were placed on the same plate, i.e. the surface embedded receiver on top of the fully embedded receiver, as shown in Fig. 2. The placement ensures that the test is accurate as both sensors receive the same event. Initially, concerns were raised regarding the potential impact of placing the surface embedded receiver on top of the fully embedded receiver. However, after conducting multiple tests before and after surface embedding, the variation in response primarily fell within the error margin of the testing machine and hence was disregarded. The fully embedded and surface embedded actuators were placed on separate plates to avoid complications when pulsing, as seen in Fig. 2.

3.1. TGP pulse generator and PLB

The findings obtained from pulsing using the surface embedded actuator revealed that the fully embedded receiver had a higher amplitude than the surface embedded receiver, as seen in Fig. 3A and B. However, the increased sensitivity is inconclusive as the difference of 2 dB can be attributed to the error from the machine, i.e. ± 1 dB from each

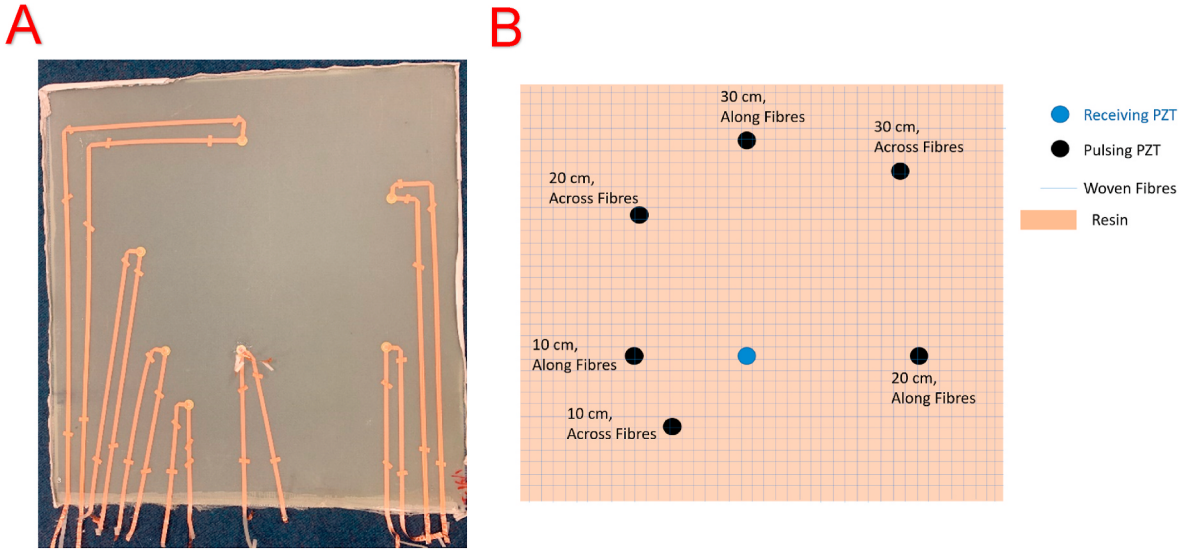

Fig. 1. (A) The cured plate after manufacturing (B) sensor's configuration illustration.

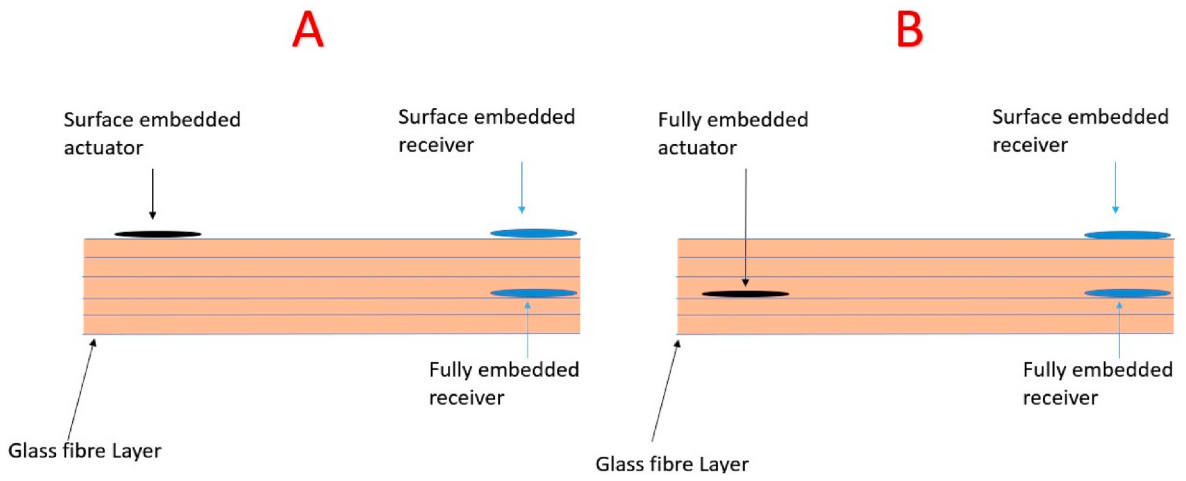

Fig. 2. The test setup for (A) plates 1 and 2 (B) plates 3 and 4.

Table 1
Materials used for manufacturing the glass fibre plates.

Epoxy Resin	RS-M135
Hardener	RS-MH137
Fibres	Glass woven roving 600 gsm plain weave

receiver. The difference in sensitivity was greater than 2 dB in certain conditions, such as at 20 and 30 cm in Fig. 3B. However, it is inconclusive as plate 1, Fig. 3A, produced different results. On the other hand, the fully embedded actuators showed comparable responses from both receivers, as shown in Fig. 3C and D. That is, the amplitude of the receivers was similar when pulsing using the fully embedded actuator and the surface embedded actuator, around 76 dB at 10 cm. A similar trend

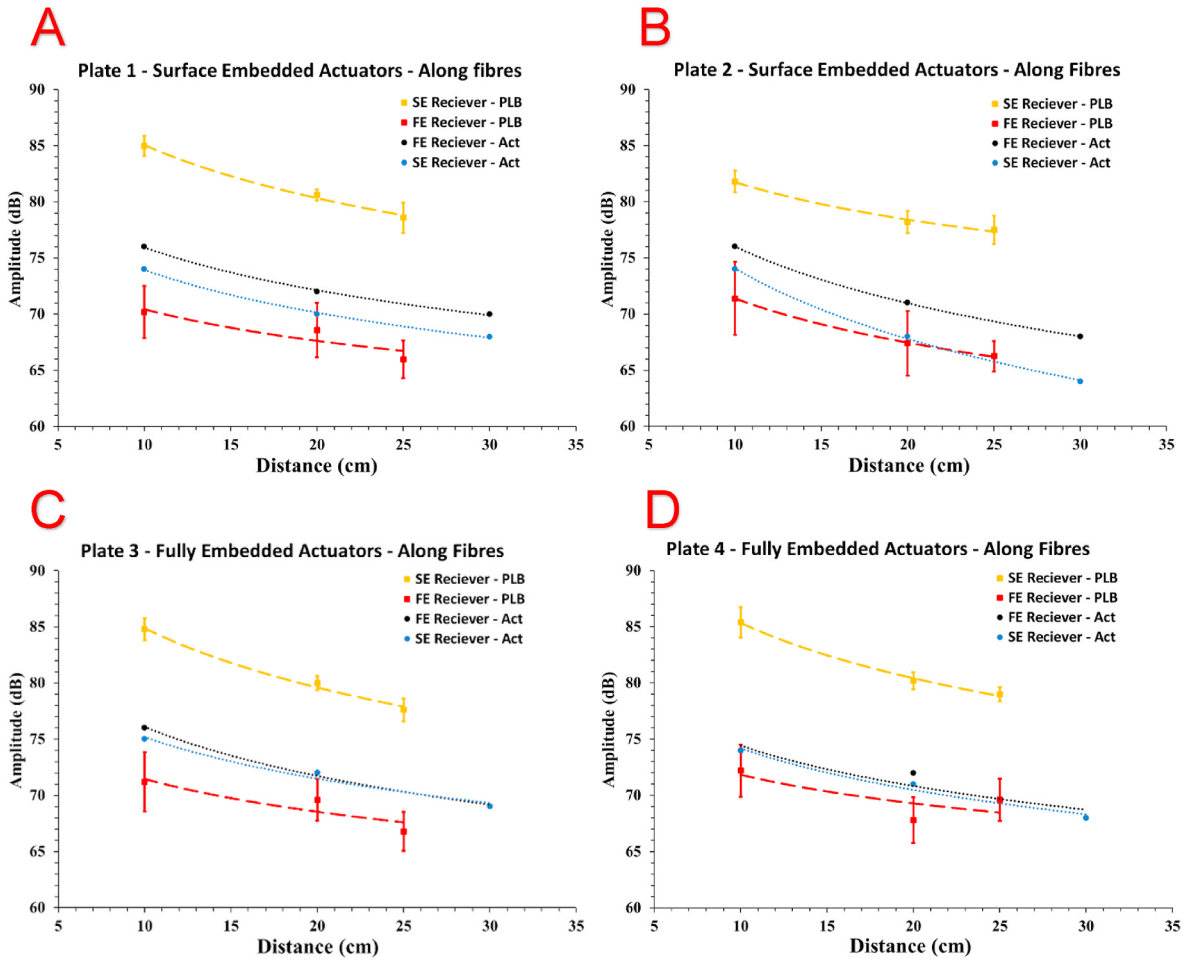

Fig. 3. The attenuation of surface embedded (SE) and fully embedded (FE) PZT receivers along fibres utilising the PLB method (A and B) and surface embedded actuators - Act (C and D) and fully embedded actuators - Act.

was recorded when testing across the fibres, as seen in Fig. 4C and D. A noticeable difference was observed when testing the attenuation along and across the fibres, which could stem from various factors, as elaborated later. No apparent difference can be observed when comparing the amplitude difference between pulsing from the surface or fully embedded actuator. Based on the actuator method results, it could have been concluded that the location of the crack does not significantly affect the sensitivity with respect to the receiver's location. This implies that the receiving sensor's sensitivity is not significantly affected by the crack's initiation location (surface or from within). However, this was not the case upon utilising the second signal-generating method (PLB).

The pencil lead-breaking method was used to generate an acoustic emission signal by breaking the pencil on the surface of the plate. Unlike the actuator method, a significant difference was evident between the surface embedded receiver and the fully embedded receiver when utilising the PLB for generating a test signal, as seen in Figs. 3 and 4. The results remained evident despite the receiver's data variability (error bars). The PLB was performed on each plate individually, with a total of 5 tests conducted, and subsequently, an average of the results was recorded. The results show that the surface embedded receiver had a much higher amplitude than the fully embedded receiver, i.e. the fully embedded receiver's performance degraded. The results were consistent along and across fibres. A significant difference of approximately 10–15 dB was observed when comparing the responses of both receivers using the PLB method. The PLB test attenuation was limited to 25 cm compared to 30 cm with the actuator method due to the presence of the actuating sensor at 30 cm.

Even though the surface and embedded receivers responded to the same PLB hit, the variations (error bars) were different, as seen clearly in Fig. 3B. When applying the PLB method, the variation associated with the fully embedded receiver was higher than the surface embedded receiver when testing along fibres (Fig. 3) but lower when testing across fibres(Fig. 4). The propagation path of the wave is affected by the fibres; as a result, the sound spreads unevenly [25]. The lower amplitude associated with testing across fibres compared to along fibres may be attributed mainly to the fibre alignment and different travelling mediums. That is, testing across the fibres could force the wave to travel across multiple fibre strands compared to a single fibre strand when along the fibres. Also, as the wave travels across the fibres, it will encounter two different mediums: resin and glass fibre. The polymer's (resin) viscoelastic nature results in thermoelastic dissipation, making it more susceptible to attenuation [26].

The pencil lead-breaking method shows that the number of plates tested is adequate to ensure the validity of the results. That is, the pencil lead-breaking method was performed on all the plates individually, and the results were similar. Hence, the effect of the sensor's intrinsic differences, if any, is minimal.

The frequencies obtained from the PLB method and the PZT actuating method were significantly different, as evident in Fig. 5, Figs. 6 and 7. The frequency response of the fully embedded and surface embedded receivers is similar when testing using the PLB method peaking at around 21 kHz, as seen in Fig. 5. Even though both sensors received the same wave, the peak frequency did not always perfectly match. The frequencies acquired through the PLB method primarily fell within the range of 1 kHz–50 kHz.

On the other hand, when testing using the surface embedded

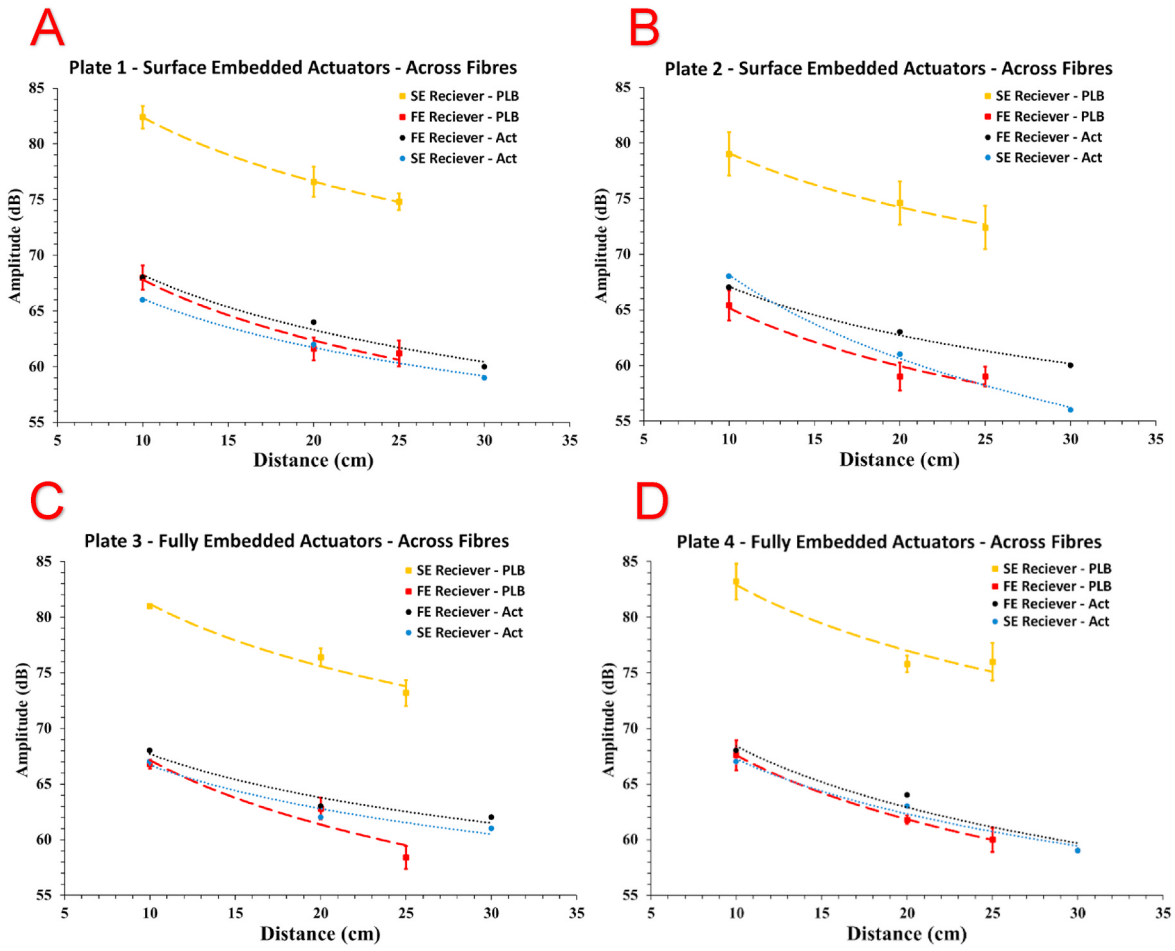

Fig. 4. The attenuation of surface embedded (SE) and fully embedded (FE) PZT receivers across fibres utilising the PLB method (A and B) and surface embedded actuators - Act (C and D) and fully embedded actuators - Act.

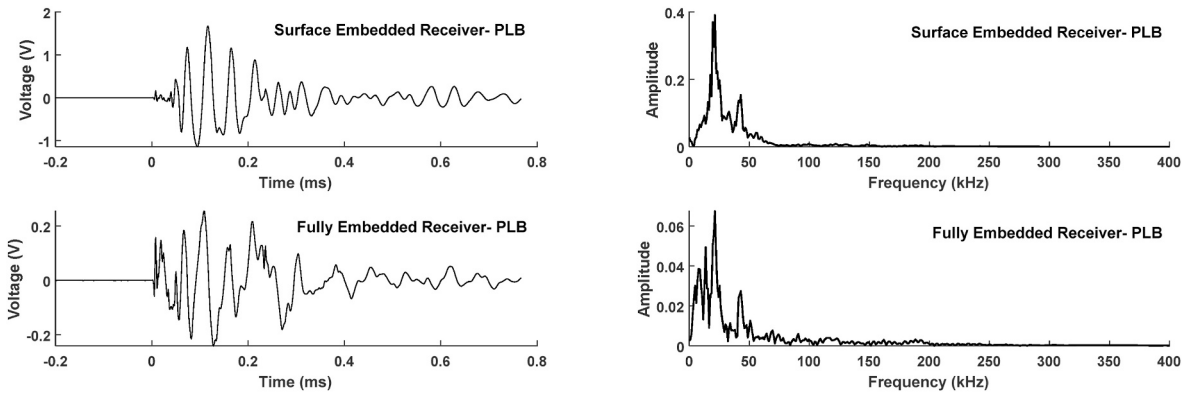

Fig. 5. Comparison of time domain (left) and frequency domain (right) responses utilising the pencil lead breaking method (PLB) at 10 cm distance along fibres for (top) surface embedded receiver (bottom) fully embedded receiver.

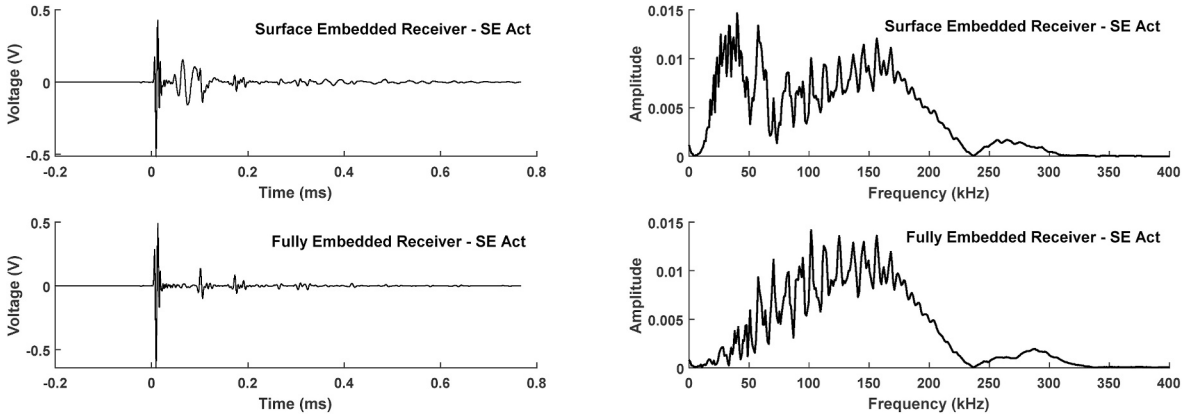

Fig. 6. Comparison of time domain (left) and frequency domain (right) responses utilising the surface embedded (SE) actuator at 10 cm distance along fibres for (top) surface embedded receiver (bottom) fully embedded receiver.

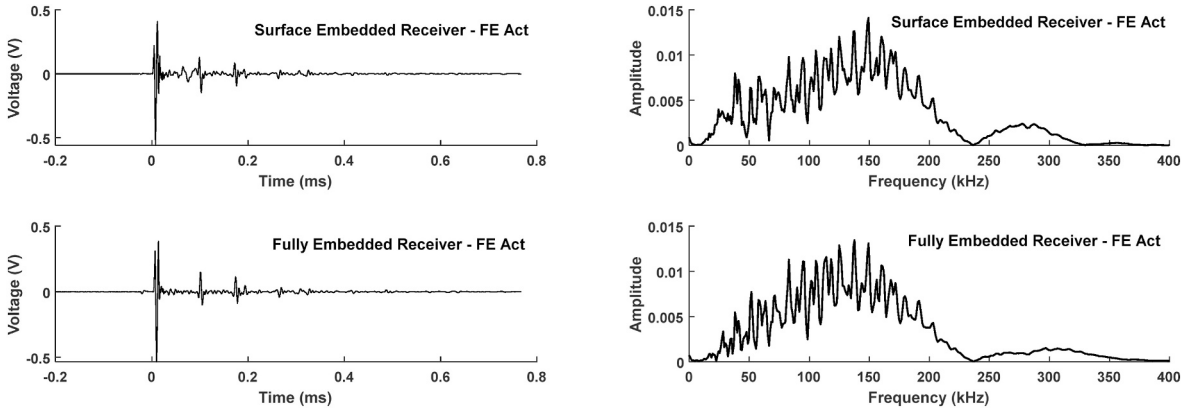

Fig. 7. Comparison of time domain (left) and frequency domain (right) responses utilising the fully embedded (FE) actuator at 10 cm distance along fibres for (top) surface embedded receiver (bottom) fully embedded receiver.

actuators, the frequency response of the receivers was different, as evident in Fig. 6. The fully embedded receiver's frequency response was broad (around 35–240 kHz) with a secondary peak between 240 and 325 kHz. On the other hand, the surface embedded receiver had an initial peak between 5 and 50 kHz. Beyond 50 kHz, it followed a similar trend as the fully embedded receiver. The initial peak between 5 and 50 kHz did not significantly affect the amplitude, i.e. both receivers' amplitude was similar.

The surface and the fully embedded receivers responded similarly when the signal was generated using the fully embedded actuator, as seen in Fig. 7. Both recorded signals had a similar trend to the fully embedded receiver signal when the surface embedded actuator was utilised. Also, the time domain signals of both receivers were similar.

The time domain signal using the surface actuating method differed significantly from the PLB method. The time domain signal of the actuating method showed secondary peaks with both receivers, as seen in Figs. 6 and 7. The possibility that the secondary hits and beyond are reflections from the plate edges is possible, even though measures were taken to prevent reflection. Measures include placing tacky tape on the plate edges as well as placing the sensors away from the edge, as seen in

Fig. 1. However, the secondary peaks are insignificant and can be disregarded due to their low amplitude compared to the main peak.

The predominant wave generated using the two methods is the anti-symmetric wave (A_0) based on the location of the signal-generating method's actuating and receiving sensors. That is, the force applied was perpendicular to the plate [26]. However, Pant's study showed that the dominant wave produced can be based on the frequency generated, even when the force was perpendicular to the plate [27]. Consequently, this area requires further investigation.

Nevertheless, the difference in wave generation mechanism, area of contact and frequency response factors can account for the divergent results obtained from the different signal generation methods. The actuating method depends on an electrical signal transmitted to the PZT, which is converted to mechanical vibration, creating a wave that transmits through the material. In comparison, the PLB method relies on breaking a brittle material (pencil lead) to induce a stress wave at the material's surface. The contact area is much smaller when testing using the PLB compared to the TGP pulse generator. The frequencies acquired from both signal generation methods exhibited variation; nevertheless, their potential influence can be tested. The disadvantage of using the TGP pulse generator is the inability to control the wave's peak frequency precisely, prompting the use of an alternative device.

3.2. Pulsing targeted frequencies

The FieldCal device produced a pulse with a pre-set frequency peak which was used to validate the frequency effects on the receiving sensor sensitivity. The sensitivity of the receiving sensor, whether surface embedded or fully embedded, was tested against surface embedded and fully embedded actuators. Four frequencies were examined, namely 30 kHz, 60 kHz, 150 kHz, and 300 kHz.

Fig. 8 shows the amplitude difference between the surface and fully embedded receiver when applying the pulse using the surface embedded actuator. The amplitude difference is calculated by subtracting the fully embedded receiver's amplitude from the surface embedded receiver's amplitude. If the amplitude difference is positive, the surface embedded receiver exhibited greater amplitude; conversely, if negative, the fully embedded receiver showed higher amplitude.Fig. 8 shows an apparent trend when comparing the amplitude against the frequency; the lower the frequency, the higher the sensitivity of the surface embedded receiver. At 30 kHz, close to the PLB method signal frequency, the amplitude difference averaged around 12 dB along and across fibres. As the frequency increased, the amplitude difference decreased. At 150 kHz, the closest frequency to the signal acquired from the TGP pulse generator, the amplitude difference was no longer noticeable. The amplitude difference acquired at 30 and 150 kHz roughly aligns with the results of the PLB and TGP pulsing methods, respectively. Thus, this validation highlights the frequency significance in influencing the sensor's sensitivity when embedding.

The receivers' response along and across the fibres, induced by the surface embedded actuators, exhibited a comparable pattern. Although the fully embedded receiver had a higher sensitivity at 300 kHz along the fibres, as seen in Fig. 8(left), the increase is not evident across the fibres, Fig. 8(right). Initial results suggest the fully embedded receiver is more sensitive when the crack initiates along the fibres at 300 kHz. The difference in results along and across fibres suggests that the wave travelling path may also influence the sensor's sensitivity with respect to frequency.

The results from the surface embedded actuator suggest that the surface embedded receiver is more sensitive to surface cracks with low frequencies (30 and 60 kHz), both along and across fibres. However, with surface cracks with midrange frequency (150 kHz), the sensitivity of both receivers is similar along and across fibres. The fully embedded receiver is more sensitive than the surface embedded receiver when high frequency (300 kHz) is aligned along the fibres. However, if the high-frequency surface crack is aligned across the fibres, both receivers sensitivity is similar.

The amplitude difference at 30 kHz dropped to around 6 dB using the fully embedded actuators along the fibres, as seen in Fig. 9(left). Testing at 30 kHz using the fully embedded actuator is similar to testing using the pencil lead-breaking method but within the laminate. Beyond 30 kHz, the results indicate that the amplitude difference between both receivers is minimal (less than 2 dB), except for a few anomalies. On the other hand, when testing using the fully embedded actuators across the fibres, Fig. 9(right), the receiver's amplitude difference is around 2 dB across all the frequencies tested, even 30 kHz. A 2 dB difference is considered insignificant due to the detection system's accuracy.

The results obtained from the fully embedded actuators reveal that the surface embedded receiver displays increased sensitivity solely to cracks originating from the composite's centre along the direction of the fibres, particularly at a frequency of 30 kHz. At all other frequencies (60, 150 and 300 kHz) along and across fibres, the sensitivity of both receivers is similar to cracks originating from the centre of the composite. Further investigation is needed to elucidate the cause behind the disparate outcomes observed during testing along and across the fibres.

3.3. The embedding process effect

Although the frequency sensitivity of the receiving PZT is not documented, the surface and fully embedded receiving PZT's were identical, implying that both exhibit matching frequency responses. For example, if the surface embedded PZT had a higher sensitivity response

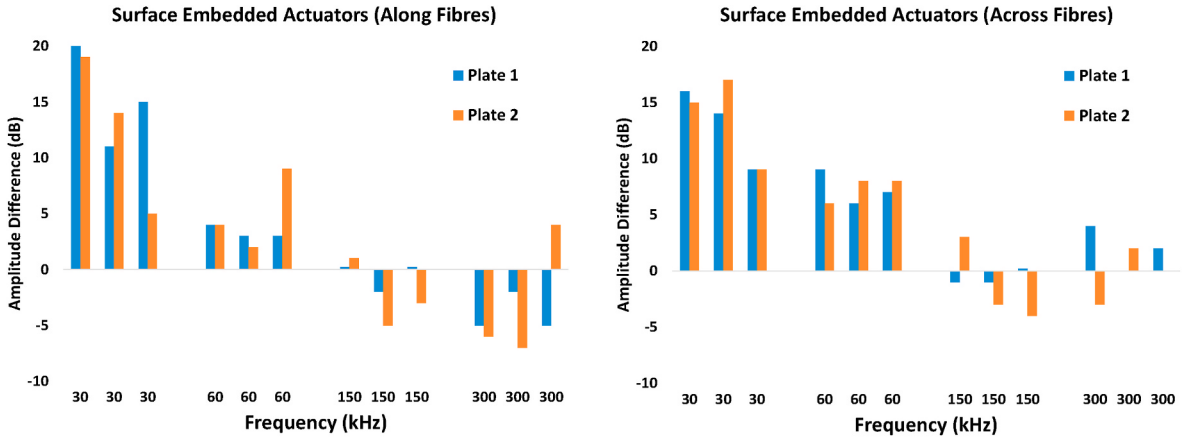

Fig. 8. The amplitude difference between the surface and fully embedded receivers (SE - FE) based on the surface embedded actuator at four frequencies, (left) along fibres (right) across fibres.

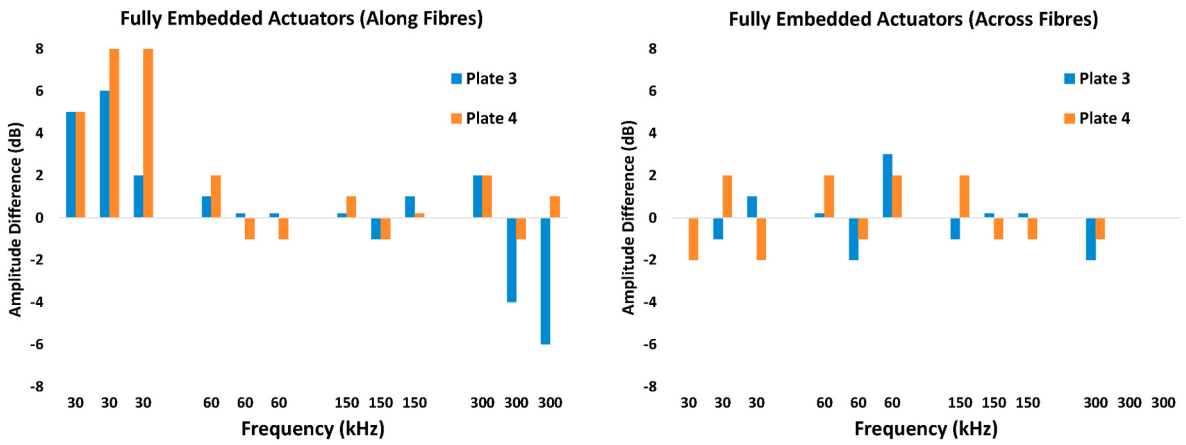

Fig. 9. The amplitude difference between the surface and fully embedded receivers (SE - FE) based on the fully embedded actuators at four frequencies (left) along fibres (right) across fibres.

at 50 kHz, the fully embedded should have a higher sensitivity at 50 kHz. Additionally, the PZT sensor demonstrated sensitivity within the tested frequency range, as the AE machine software successfully received and displayed the frequency spectrum containing the peaks of each pulse. However, the frequency sensitivity of the receiving sensor may have shifted due to the embedding process (the pressure and surrounding material). The idea of frequency sensitivity transition due to the embedding process can be argued to have no effect using the PLB method data, which shows that a similar peak produced different amplitudes. However, when viewing the fully embedded actuating data, both receivers had a similar amplitude at a similar frequency response. Hence, the embedding process might have influenced the frequency sensitivity at specific frequencies.

The variation in results between the signal-generating methods is predominantly attributed to the frequency. However, it is essential to note that other factors, such as the sensor properties and material thickness can also contribute to this phenomenon. For example, if another receiving sensor is used, could the frequency transition occur at another frequency? Also, how does the change in material thickness affect the signal's amplitude with respect to the sensor's placement? If amplitude variation is exclusively dependent on frequency, it is not advisable to fully embed the acoustic emission sensor in composites because initial crack formation occurs at low frequencies. When a glass fibre composite fails, the initial failing mechanisms, depending on the situation, can be matrix cracking or fibre-matrix cracking, which occur at a relatively low frequency, as seen in Table 2. Even though initial failure can occur at 300 kHz, more hits are likely at frequencies lower than 300 kHz. On the other hand, fibre fracture occurs at high frequencies, where the embedded sensor might have a higher sensitivity depending on the crack initiation point. However, detecting earlier failure events (at lower frequencies) where the fully embedded receiver is less sensitive or as sensitive is preferable over high-frequency events that indicate critical structural conditions.

Table 2
The frequency acquired from glass fibre/epoxy matrix composite failure mechanisms, adapted from Ref. [28].

Reference	Thickness (mm)	Frequency Response (kHz)			
		Matrix Cracking	Fibre-Matrix Cracking	Delamination	Fibre Fracture
[11]	2.78	90–110	–	130–200	250–280
[12]	4	62.5–125	125–187.5	–	187.5–250
[13]	5	100–190	200–320	–	380–430
[14]	4.8	60–180	190–250	–	350–500
[15]	4.8	11–93	82–210	–	160–281

The drawbacks linked to the potential degradation of mechanical properties due to sensor embedding and manufacturing challenges overshadow the benefit of increased sensitivity at specific frequencies. The potential benefit of protecting sensors through embedding, which provides a shield from external conditions, can positively impact the viability of the embedding approach. However, further research is required in this aspect.

This study represents the initial phase of exploring sensor sensitivity based on location, which was accomplished using artificial acoustic emission sources. The artificial acoustic emission sources are valid and have been used elsewhere [6,27]. However, the next step is to demonstrate the behaviour using AE arising from actual failure.

4. Conclusion

The placement of the receiving sensors on the same test plate ensured that the results could be accurately compared, avoiding variability from the composite plate due to processing. The receiving sensor's sensitivity (registered amplitude) varied with the different signal-generating methods. The PLB method showed that the fully embedded receiver registered lower amplitude than the surface embedded receiver, proving lower sensitivity when embedding. On the other hand, PZT actuation utilising the TGP pulse generator showed that the receiving sensor's sensitivity variation was inconclusive and was, therefore, considered similar with both surface and fully embedded actuators. That is, the PLB method results showed that embedding AE sensors degrades their performance compared to the TGP pulse generator, which showed that performance is unchanged. The discrepancy in results among the testing methods was thought to stem from the acoustic signal frequency generated by each method. That is, the PLB frequency response peaked at a low frequency (around 21 kHz) compared to the TGP pulse generator, which mostly peaked at around 150 kHz.

The FieldCal was employed to verify the sensor's sensitivity concerning different frequencies. It was found that the receiving sensor's sensitivity varied when utilising different frequencies. In most cases, the surface embedded receiver had higher sensitivity at 30 kHz (near the PLB peak) compared to comparable behaviour at 150 kHz(near the TGP peak). Also, the location of the AE source (surface or fully embedded) affected the amplitude difference between the receiving sensors, depending on the frequency.

The fully embedded sensor can, at a specific condition, detect high frequency signals better than the surface embedded sensor. However, early failure mechanisms, such as matrix cracking, are usually lower frequency events where the fully embedded sensor was not proven to have any advantage over the surface mounted sensor.

Furthermore, the AE signal's amplitude was affected by the wave

travelling path. That is, AE wave travelling across the fibres exhibited lower amplitude than along the fibres, which was thought to be due to the different mediums and fibre orientation.

Disclosure

During the preparation of this work the author (Noor Salam Ghadarah) used AI tools to improve the structure and wording of the sentences. After using this tool/service, the author reviewed and edited the content as needed and take full responsibility for the content of the publication.

Declaration of competing interest

The authors declare that they have no known competing financial interests or personal relationships that could have appeared to influence the work reported in this paper.

Data availability

Data will be made available on request.

References

[1] Fraunhofer Institute for Ceramic Technologies and Systems IKTS, Acoustic emission testing on composite structures for damage detection - Fraunhofer IKTS. https://www.ikts.fraunhofer.de/en/departments/electronics_microsystems_biomedicine/condition_monitoring_non-destructive_testing/acoustic_emission_testing_on_composite_structures_for_damage_detection.html. (Accessed 17 June 2023).

[2] M.A. Rumsey, J.A. Paquette, Structural Health Monitoring of Wind Turbine Blades, 2008.

[3] V. Giurgiutiu, Impact and Acoustic Emission Monitoring for Aerospace Composites SHM. Structural Health Monitoring of Aerospace Composites, Academic Press, 2016, pp. 317–394, https://doi.org/10.1016/B978-0-12-409605-9.00009-X.

[4] L. Srivastava, L. Krishnanand, N. Kishore Nath, C.K. Hirwani, M.R.M. Babu, Online structural integrity monitoring of high-performance composite rocket motor casing, Mater. Today: Proc. 56 (2022) 1001–1009, https://doi.org/10.1016/J.MATPR.2022.03.230. Elsevier.

[5] C. Wilkerson, Acoustic Emission Monitoring of the DC-XA Composite Liquid Hydrogen Tank during Structural Testing, 1996.

[6] S. Sikdar, P. Mirgal, S. Banerjee, W. Ostachowicz, Damage-induced acoustic emission source monitoring in a honeycomb sandwich composite structure, Compos. B Eng. 158 (2019) 179–188, https://doi.org/10.1016/j.compositesb.2018.09.071.

[7] F. Ciampa, M. Meo, A new algorithm for acoustic emission localization and flexural group velocity determination in anisotropic structures, Compos. Appl. Sci. Manuf. 41 (12) (2010) 1777–1786, https://doi.org/10.1016/j.compositesa.2010.08.013.

[8] M.J. Eaton, R. Pullin, K.M. Holford, Acoustic emission source location in composite materials using Delta T Mapping, Compos. Appl. Sci. Manuf. 43 (6) (2012) 856–863, https://doi.org/10.1016/j.compositesa.2012.01.023.

[9] S. Masmoudi, A. El Mahi, S. Turki, Use of piezoelectric as acoustic emission sensor for in situ monitoring of composite structures, Compos. B Eng. 80 (2015) 307–320, https://doi.org/10.1016/J.COMPOSITESB.2015.06.003. Elsevier.

[10] S. Masmoudi, A. El Mahi, S. Turki, R. El Guerjouma, Structural health monitoring by acoustic emission of smart composite laminates embedded with piezoelectric sensor, Springer Heidelberg, Lecture Notes in Mechanical Engineering 1 (2013) 307–314, https://doi.org/10.1007/978-3-642-37143-1_37. Accessed: 10 November 2020).

[11] R. Asokan, V. Arumugam, C. Santulli, S. Kumar, A. Stanley, Investigation of the strength of the failure modes in GFRP laminates using acoustic emission monitoring, Int. J. Polym. Technol. 3 (2011).

[12] N. Beheshtizadeh, A. Mostafapour, S. Davoodi, Three point bending test of glass/epoxy composite health monitoring by acoustic emission, Alex. Eng. J. 58 (2) (2019) 567–578, https://doi.org/10.1016/J.AEJ.2019.03.006. Elsevier.

[13] Fotouhi M., Heidary H., Ahmadi M., Pashmforoush F. Characterization of composite materials damage under quasi-static three-point bending test using wavelet and fuzzy C-means clustering. https://doi.org/10.1177/0021998311425968. SAGE PublicationsSage UK: London, England; 1 February 2012; 46(15): 1795–1808. Available at: DOI:10.1177/0021998311425968 (Accessed: 25 December 2022).

[14] M. Nikbakht, J. Yousefi, H. Hosseini-Toudeshky, G. Minak, Delamination evaluation of composite laminates with different interface fiber orientations using acoustic emission features and micro visualization, in: Composites Part B: Engineering, vol. 113, Elsevier, 2017, pp. 185–196, https://doi.org/10.1016/J.COMPOSITESB.2016.11.047.

[15] W. Zhou, W Zhao, Y Zhang, Z Ding, Cluster analysis of acoustic emission signals and deformation measurement for delaminated glass fiber epoxy composites, Compos. Struct. 195 (2018) 349–358, https://doi.org/10.1016/J.COMPSTRUCT.2018.04.081. Elsevier.

[16] X.P. Qing, S.J. Beard, A. Kumar, T.K. Ooi, F.-K. Chang, Built-in sensor network for structural health monitoring of composite structure, Sage PublicationsSage CA: Thousand Oaks, CA, J. Intell. Mater. Syst. Struct. 18 (1) (2007) 39–49, https://doi.org/10.1177/1045389X06064353. Accessed: 12 November 2020).

[17] I.M. De Rosa, F. Sarasini, Use of PVDF as acoustic emission sensor for in situ monitoring of mechanical behaviour of glass/epoxy laminates, Polym. Test. 29 (6) (2010) 749–758, https://doi.org/10.1016/j.polymertesting.2010.04.006. Elsevier.

[18] C. Tuloup, W. Harizi, Z. Aboura, Y. Meyer, Integration of piezoelectric transducers (PZT and PVDF) within polymer-matrix composites for structural health monitoring applications: new success and challenges, Taylor and Francis Ltd, Int. J. Soc. Netw. Min. 11 (4) (2020) 343–369, https://doi.org/10.1080/19475411.2020.1830196. Accessed: 13 April 2021).

[19] S. Masmoudi, A. El Mahi, S. Turki, Fatigue behaviour and structural health monitoring by acoustic emission of E-glass/epoxy laminates with piezoelectric implant, Elsevier Ltd, Appl. Acoust. 108 (2016) 50–58, https://doi.org/10.1016/J.APACOUST.2015.10.024 (Accessed: 19 January 2023).

[20] C. Caneva, I.M. De Rosa, F. Sarasini, Monitoring of impacted aramid-reinforced composites by embedded PVDF acoustic emission sensors, John Wiley & Sons, Ltd, Strain 44 (4) (2008) 308–316, https://doi.org/10.1111/j.1475-1305.2007.00374.x. Accessed: 17 December 2020.

[21] S. Masmoudi, A. El Mahi, S. Turki, R. El Guerjouma, Mechanical behavior and health monitoring by Acoustic Emission of unidirectional and cross-ply laminates integrated by piezoelectric implant, Appl. Acoust. 86 (2014) 118–125, https://doi.org/10.1016/J.APACOUST.2014.04.011. Elsevier Ltd.

[22] S. Masmoudi, A. El Mahi, R. El Guerjouma, Mechanical behaviour and health monitoring by acoustic emission of sandwich composite integrated by piezoelectric implant, Elsevier Ltd, Compos. B Eng. 67 (2014) 76–83, https://doi.org/10.1016/J.COMPOSITESB.2014.05.032. Accessed: 23 January 2023.

[23] S. Masmoudi, A. El Mahi, S. Turki, Effect of piezoelectric implant on the structural integrity of composite laminates subjected to tensile loads, Springer Netherlands, Appl. Compos. Mater. 24 (1) (2017) 39–54, https://doi.org/10.1007/S10443-016-9513-4. Accessed: 23 January 2023).

[24] G. Seychal, E. Ramasso, P. Le Moal, G. Bourbon, X. Gabrion, V. Placet, Towards in-situ acoustic emission-based health monitoring in bio-based composites structures: does embedment of sensors affect the mechanical behaviour of flax/epoxy laminates?, in: Composites Part B: Engineering, vol. 236 Elsevier, 2022, 109787 https://doi.org/10.1016/J.COMPOSITESB.2022.109787.

[25] M. Sause, M. Hamstad, Acoustic Emission Analysis. Comprehensive Composite Materials II, Elsevier, 2017, pp. 291–326, https://doi.org/10.1016/B978-0-12-803581-8.10036-0. Accessed: 20 December 2022).

[26] C.J. Hellier, The Signal-Shaping Chain, third ed., McGraw-Hill Education, New York, 2020. Available at: https://www.accessengineeringlibrary.com/content/book/9781260441437/toc-chapter/chapter10/section/section23.

[27] S. Pant, J. Laliberte, M. Martinez, Structural Health Monitoring (SHM) of Composite Aerospace Structures Using Lamb Waves, 2013.

[28] N. Ghadarah, D. Ayre, A review on acoustic emission testing for structural health monitoring of polymer-based composites, Sensors (2023), https://doi.org/10.3390/s23156945.

https://dspace.org/

A comparative analysis of acoustic emission sensor embedding in glass fibre composite

Ghadarah, Noor Salam; Ayre, David

2024-03-01
Elsevier
https://doi.org/10.1016/j.compscitech.2023.110392
Ghadarah N, Ayre D. (2024) A comparative analysis of acoustic emission sensor embedding in glass fibre composite. Composites Science and Technology, Volume 247, March 2024, Article number 110392

Downloaded from a DSpace repository. https://dspace.org/